A Hybrid Phase Shift-Pulsewidth Modulation and Asymmetric Selective Harmonic Current Mitigation-Pulsewidth Modulation Technique to Reduce Harmonics and Inductance of Single-Phase Grid-Tied Cascaded Multilevel Converters

Amirhossein Moeini [ID], *Member, IEEE*, Shuo Wang [ID], *Fellow, IEEE*, Boyi Zhang, *Student Member, IEEE*, and Le Yang [ID], *Student Member, IEEE*

Abstract—In this article, a low-frequency hybrid modulation technique which is composed of a phase shift-pulsewidth modulation (PS-PWM) and an asymmetric selective harmonic current mitigation-PWM (ASHCM-PWM) are proposed for cascaded multilevel converters to meet the harmonic limit of IEEE 519 2014. In the proposed technique, the harmonics within the concerned frequency range due to PS-PWM are reduced by the ASHCM-PWM so that the cascaded H-bridge (CHB) converter can meet IEEE 519 harmonic limit. The equation set which helps a grid-tied CHB converter meet both harmonic limit and total demand distortion, is developed. The design technique for critical parameters, such as the inductance and the switching frequency of the proposed hybrid modulation technique, is developed. Simulation and experiments are conducted on a single-phase 3-cell 7-level grid-tied CHB converter to validate the proposed technique.

Index Terms—Asymmetric selective harmonic current mitigation-pulsewidth modulation (SHCM-PWM), grid-tied cascaded H-bridge (CHB) converters, low-frequency modulation technique, phase shift-pulsewidth modulation (PS-PWM).

I. INTRODUCTION

MULTILEVEL cascaded H-bridge (CHB) converters have several advantages over conventional two-level converters such as low-total harmonic distortion and high-efficiency [1] and [2]. The modulation technique used on the multilevel converters should have high-efficiency, high-dynamic performance,

and meet power quality standards [2]. Also, the modulation technique should be able to inject or absorb active and reactive power from the power grid [1] to achieve various grid support functionalities.

The modulation techniques of a grid-tied CHB converter is classified based on the switching frequency of the converter [2]: a) low-frequency modulation techniques such as the selective harmonic elimination-PWM (SHE-PWM) [3], and the selective harmonic mitigation-PWM (SHM-PWM) [4]; b) high-frequency modulation techniques such as the phase shift-pulsewidth modulation (PS-PWM) [5].

Low-frequency modulation techniques can control the low-order harmonics of the voltage of a multilevel converter to meet the power quality standards by controlling switching angles based on the Fourier series transcendental equations [2]–[4]. The SHE-PWM, which can be implemented on the multilevel inverters, was proposed in [6]. SHE-PWM technique was used on the CHB active rectifier in [3]. The advantage of the SHE-PWM is high-efficiency due to low-number of switching transitions [2].

The SHM-PWM technique was first introduced in [4]. In this technique, instead of eliminating the low-order voltage harmonics of a CHB, the harmonics are mitigated to be lower than the limits of power quality standards [4]. As discussed in [4], the number of voltage harmonics that can be mitigated using the SHM-PWM technique is higher (depending on the best operating point and the grid-code of power quality standards) than the number of harmonics that can be eliminated using SHE-PWM technique when they have the same number of switching transitions. Also, both of them target to reduce voltage harmonics only so they could not guarantee to meet current harmonics limits. A new selective harmonic mitigation-pulse amplitude modulation was proposed in [8] to eliminate the triplen harmonics of the single-phase CHB converter by controlling the dc-link voltages of the CHB cells using redundant converters. The low-order nontriplen harmonics of the CHB voltage in [8] are mitigated by controlling the switching angles to meet the harmonic voltage requirements. However, this technique needs to change the dc-link voltages of all CHB cells for different modulation indices which can increase the complexity and the

cost of the converter. Recently, a fault-tolerant asymmetric selective harmonic elimination-PWM (asymmetric SHE-PWM) technique was proposed in [9] for a three-phase CHB converter by generating a balanced ac voltage when one of the cells fails.

The PS-PWM technique is one of the most commonly used modulation techniques in industry. Although PS-PWM technique can control the fundamental in a wide range and it is very simple to implement, this technique cannot achieve the best harmonic performance among all available modulation techniques with low switching frequencies and small coupling inductance. The PS-PWM technique generates the CHB voltage by comparing the high-frequency carrier waveform with the ac reference [5]. In [5], different methods to generate the CHB voltage with the PS-PWM technique were discussed. The harmonic voltage equation of the PS-PWM technique is derived in [5]. It was proven that most of the significant harmonics of the PS-PWM are located within the sidebands of carrier fundamental and harmonics [5]. As a result, the switching frequency of the PS-PWM technique must be high enough to eliminate low-order harmonics in the CHB voltage. The high switching frequency leads to higher switching losses and lower power efficiency than the low-frequency modulation techniques.

In [10], a low-frequency selective harmonic current mitigation-PWM (SHCM-PWM) technique was proposed to directly control the current harmonics of a CHB converter and meet current harmonic standards instead of eliminating or mitigating voltage harmonics as used in SHE-PWM or SHM-PWM techniques. As proven in [10], with the same number of switching transitions, the SHCM-PWM technique can control a higher number of current harmonics than SHE-PWM and SHM-PWM techniques at the point of common coupling (PCC) with a smaller passive filter than SHE-PWM and SHM-PWM techniques. In [11], the advantages of current harmonic mitigation technique over conventional SHE-PWM technique are presented for a grid-tied three-phase converter. In [12] a combined SHE-PWM and THD minimization technique was proposed to achieve a wide solution range for the minimization techniques.

Although low-frequency modulation techniques with quarter-wave symmetry can control the magnitudes of the voltage harmonics of the CHB converter [10], it cannot control the phases of the voltage harmonics of the CHB converter [2]. On the other hand, low-frequency modulation techniques with half-wave symmetry can control both magnitudes and phases of the voltage harmonics of grid-tied converters [2].

Hybrid modulation technique helps grid-tied CHB converters to achieve high performance [13]–[15]. It is especially useful for the applications with unequal loads or generation units (such as photovoltaic applications) [17]. As discussed in [23], for the cells with high power, the low frequency modulation techniques can be applied to reduce the total switching power loss because the switching power loss is proportional to switching frequencies, switching currents, and switching voltages. On the other hand, for the cells with low power, the high switching frequency modulation techniques such as PS-PWM technique [14] can be applied to improve dynamic response. The existing literature did not investigate how to meet IEEE 519-2014 Standard [16] for the current harmonics with the hybrid technique.

The technique in [10] did not discuss how to improve the dynamic response of the grid-tied CHB converters when the low-frequency SHCM-PWM technique is used. As discussed in [2], the dynamic response of the low-frequency modulation technique is weak. In [18], a hybrid modulation technique is
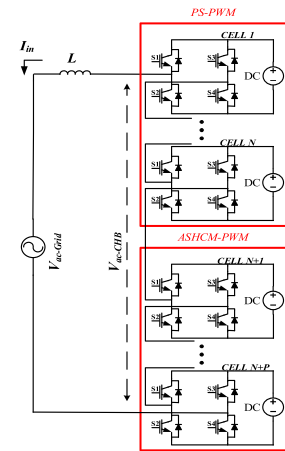

Fig. 1. $N + P$-cell CHB converter tied to a power grid.

proposed to improve the dynamic performance of grid-tied converters by applying SHCM-PWM technique during steady state and PS-PWM technique during dynamic transition [18]. However, [18] cannot simultaneously use both PS-PWM and SHCM-PWM during both steady-state and dynamic transition when unequal loads or generation units are connected to the cascaded cells of the converters.

This article will focus on two contributions.

1) A hybrid PS-PWM and ASHCM-PWM technique is developed to reduce the switching frequency and inductance of the PS-PWM technique and meet the limits of IEEE 519 2014. The voltage harmonics due to the PS-PWM technique are mitigated with the harmonics generated from the low-frequency ASHCM-PWM technique. Consequently, the switching frequency is reduced. Moreover, a general equation set for the proposed hybrid PS-PWM and ASHCM-PWM technique is derived based on the equations of the PS-PWM and ASHCM-PWM techniques.

2) Techniques are developed for the design of critical parameters such as the coupling inductance and the switching frequency of the proposed hybrid modulation technique. The proposed technique increases power efficiency, reduces inductance, meets the limits of IEEE 519, and achieve four-quadrant operation for grid-tied CHB converters.

II. PROPOSED HYBRID PS-PWM AND ASYMMETRIC SHCM-PWM TECHNIQUE

In Fig. 1. a hybrid modulation technique is proposed for an $N + P$-cell CHB converter to achieve both high-efficiency and harmonic mitigation. N cells are modulated with the PS-PWM to achieve better dynamic performance than low-frequency modulation techniques [18] and P cells are modulated with the ASHCM-PWM to help meet current harmonic limits. The CHB has a voltage of $v_{\text{ac-CHB}}(t)$ and the CHB's ac current $i_{\text{in}}(t)$ is injected into the power grid $v_{\text{ac-Grid}}(t)$. The dc link voltage of each cell is V_{dc}. L is the coupling inductance between $v_{\text{ac-CHB}}(t)$ and $v_{\text{ac-Grid}}(t)$.
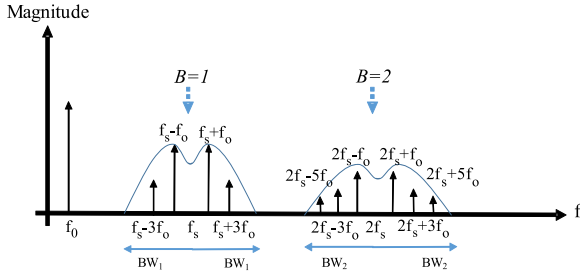
Fig. 2. Harmonic magnitudes and envelope of the PS-PWM.

A. PS-PWM Technique

Holmes and Lipo [5] derived the magnitudes and phases for the harmonic voltages of N HB cells with the PS-PWM

$$
v_{\text{ac}-\text{CHB}-\text{PSPWM}}(t)
$$
$$
= NV_{\text{dc}}M\cos(\omega_o t + \theta_o)
$$
$$
+ \frac{4V_{\text{dc}}}{\pi}\sum_{B=1}^{\infty}\sum_{A=-\infty}^{\infty}\frac{1}{2B}J_{2A-1}(NB\pi M)
$$
$$
\times \sin\left((2NB+2A-1)\frac{\pi}{2}\right)
$$
$$
\times \cos(2NB\omega_c t + (2A-1)(\omega_o t + \theta_o)) \tag{1}
$$

where B and A are the baseband and sideband harmonic orders, respectively. $v_{\text{ac-CHB-PSPWM}}(t)$ is the total voltage of the N-cell CHB with the PS-PWM technique, J is the Bessel function of the first kind. $\omega_c = 2\pi f_c$ is the carrier frequency in radian and f_c is the carrier frequency in Hz. As proven in [5], the best harmonic spectra in (1) can be achieved, when the carrier frequencies of different cells of the converter have the angle displacements of (180/N). It is worth to note that (1) is correct for any number of H-bridge cells ($N = 1,2,\dots$) when there is 180°/N phase displacement between the carrier signals of the cells. As an example, when $N = 1$, only one cell uses PS-PWM and 180° phase displacement is applied to the cell itself. f_o, θ_o, and $\omega_o = 2\pi f_o$, are the frequency in Hz, phase in radian and the angular speed in radian/s of the fundamental voltage $v_{\text{ac-CHB-PSPWM}}(t)$. From (1) and Fig. 2, it can be concluded that although the magnitudes of baseband harmonics are zero, the magnitudes of the sideband harmonics of each baseband are not zero in the harmonic spectra of the PS-PWM technique. The total modulation index of the CHB converter is $M_a = M(N+P)$, where M is the average modulation index of all cells. The dc links of these CHB cells can be connected to various loads or generation units via dc/dc converters which also help regulate dc link voltage and suppress the second order voltage harmonics. By expanding sin ((2NB + 2A − 1) π/2) in (1), the following equation holds:

$$
v_{\text{ac}-\text{CHB}-\text{PSPWM}}(t)
$$
$$
= NV_{dc}M\cos(\omega_o t + \theta_o)
$$
$$
+ \frac{4V_{\text{dc}}}{\pi}\sum_{B=1}^{\infty}\sum_{A=-\infty}^{\infty}\frac{1}{2B}J_{2A-1}(NB\pi M)
$$
$$
\times \cos(NB\pi)\sin\left((2A-1)\frac{\pi}{2}\right)
$$
$$
\times \cos(2NB\omega_c t + (2A-1)(\omega_o t + \theta_o)). \tag{2}
$$

By shifting the fundamental by $-90°$ and harmonics by $-(2A-1)90°$, the second term in (2) can be further written as (3)

$$
v_{\text{ac}-\text{CHB}-\text{PSPWM}}(t)
$$
$$
= NV_{\text{dc}}M\sin(\omega_o t + \theta_o) + \frac{4V_{\text{dc}}}{\pi}
$$
$$
\times \sum_{B=1}^{\infty}\sum_{A=-\infty}^{\infty}\frac{1}{2B}J_{2A-1}(NB\pi M)\cos(NB\pi)\sin\left((2A-1)\frac{\pi}{2}\right)
$$
$$
\times \cos\left(2NB\omega_c t + (2A-1)\left(\omega_o t + \theta_o - \frac{\pi}{2}\right)\right). \tag{3}
$$

The second term in (3) consists of the harmonic components of the CHB voltage. It can be decomposed into the sine and cosine components as

$$
v_{\text{ac}-\text{CHB}-\text{PSPWM}}(t)
$$
$$
= NV_{\text{dc}}M\sin(\omega_o t + \theta_o) + \frac{4V_{\text{dc}}}{\pi}
$$
$$
\times \sum_{B=1}^{\infty}\sum_{A=-\infty}^{\infty}\frac{1}{2B}J_{2A-1}(NB\pi M)\cos(NB\pi)
$$
$$
\times \sin((2A-1)\theta_o)\cos(2NB\omega_c t + (2A-1)(\omega_o t))
$$
$$
+ \frac{4V_{\text{dc}}}{\pi}\sum_{B=1}^{\infty}\sum_{A=-\infty}^{\infty}\frac{1}{2B}J_{2A-1}(NB\pi M)\cos(NB\pi)
$$
$$
\times \cos((2A-1)\theta_o)\sin(2NB\omega_c t + (2A-1)(\omega_o t)). \tag{4}
$$

As shown in (4), the magnitudes of the sine and cosine components depend on the θ_o of the fundamental. As a result, the magnitudes of the harmonics of the PS-PWM in the conventional technique cannot be controlled if the fundamental is controlled. On the other hand, similar to the asymmetric SHE-PWM [9], the ASHCM-PWM technique can control both the magnitude and phase of each harmonic, so it is employed in the proposed hybrid modulation technique to mitigate the total harmonics to meet IEEE 519. The magnitudes of the harmonics in (4) when B is less than or equal to 2 are shown in Fig. 2(b). In Fig. 2(b), f_s is the switching frequency of $v_{\text{ac-CHB-PSPWM}}(t)$ and $f_s = 2Nf_c$. The bandwidth BW_B of the Bth order baseband in Fig. 2(b) is given by Carlson's rule [14]

$$
BW_B \approx 2(NMB\pi + 2)f_0. \tag{5}
$$

In Fig. 2(b), the overlap of BW_1 and f_0 should be avoided because switching harmonics will influence the fundamental. At the same time, f_s which is equal to $2Nf_c$, should be as low as possible to minimize switching power loss. To achieve both goals, the following condition should be met:

$$
f_s - BW_1 > f_0 \Rightarrow f_s > f_0 + BW_1. \tag{6}
$$

B. Asymmetric SHCM-PWM Technique

For P cells that use the ASHCM-PWM in Figs. 1 and 3, if the fundamental phase of the P-cell CHB voltage $v_{\text{ac-CHB-ASHCM}}(t)$ is equal to θ_o, its Fourier series is

$$
v_{\text{ac}-\text{CHB}-\text{ASHCM}}(t) = \sum_{h=1}^{\infty}\left(\frac{2V_{\text{dc}}}{\pi h}(-\sin(h\theta_1) + \sin(h\theta_2)\right.
$$
$$
- \cdots + \sin(h\theta_K))\cos(h\omega_o t + h\theta_o)
$$
$$
+ \frac{2V_{\text{dc}}}{\pi h}(\cos(h\theta_1) - \cos(h\theta_2) + \cdots
$$
$$
\left. - \cos(h\theta_K))\sin(h\omega_o t + h\theta_o)\right). \tag{7}
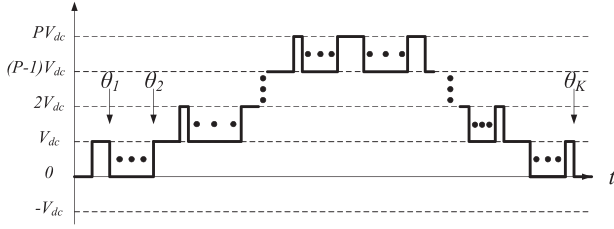$$

Fig. 3. Time-domain waveform of the ASHCM-PWM within a half-period.

where h is the harmonic order, K is the number of switching transitions in each half-period for the P-cell CHB. Because of the asymmetric waveform generated by the ASHCM-PWM in Fig. 3 has a half-wave symmetry, the even order harmonics in (7) are equal to zero. θ_1, $\theta_2, \ldots,$ and θ_K represent the switching angles of switching transitions of the ASHCM-PWM in each half-period. By expanding $\cos(h\omega_o t + h\theta_o)$ and $\sin(h\omega_o t + h\theta_o)$ in (7), (7) can be rewritten as

$$
\begin{aligned}
v_{\text{ac-CHB-ASHCM}}(t) \\
= \sum_{h=1}^{\infty} \Big(\frac{2V_{\text{dc}}}{\pi h} (-\sin(h\theta_1 - h\theta_o) + \sin(h\theta_2 - h\theta_o) \\
- \cdots + \sin(h\theta_K - h\theta_o))\cos(h\omega_o t) \\
+ \frac{2V_{\text{dc}}}{\pi h}(\cos(h\theta_1 - h\theta_o) - \cos(h\theta_2 - h\theta_o) \\
+ \cdots - \cos(h\theta_K - h\theta_o))\sin(h\omega_o t) \Big).
\end{aligned}
\tag{8}
$$

In (8), because the sine and cosine terms of the harmonics are decoupled, different from conventional techniques, both the magnitude and phase of the fundamental and low-order harmonics can be controlled by controlling the switching angles θ_1, $\theta_2, \ldots,$ and θ_K. As a result, the low-order harmonics due to the PS-PWM in N-cell CHBs can be compensated with the harmonics generated by the ASHCM-PWM in (8) by controlling the switching angles.

TABLE I
HARMONIC LIMITS OF IEEE 519 [16]

$I_{sc}/I_L{\leq}20$	<11	$11{\leq}h{<}17$	$17{\leq}h{<}23$	$23{\leq}h{<}35$	$35{\leq}h{<}50$	C_{TDD}
$C_{h\,\&\,C_{TDD}}$	4%	2%	1.5%	0.6%	0.3%	5%

C. Derivation of Equations for Hybrid PS-PWM and Asymmetric SHCM-PWM Technique

In Fig. 1, the hth order current harmonic $I_{\text{in}-h}$ can be calculated as

$$
|I_{\text{in}-h}| = \left| \frac{\begin{array}{c} V_{\text{ac-CHB-PSPWM}-h}\angle\theta_{\text{PSPWM}-h} \\ +V_{\text{ac-CHB-ASHCM}-h}\angle\theta_{\text{ASHCM}-h} \end{array}}{j\omega_o h L} \right|
\tag{9}
$$

where $V_{\text{ac-CHB-PSPWM}-h}$, $V_{\text{ac-CHB-PSPWM}-h}$, $\theta_{\text{PSPWM}-h}$ and $\theta_{\text{ASHCM}-h}$ are the magnitudes and phases of the hth order voltage harmonic due to the PS-PWM and ASHCM-PWM, respectively. $I_{\text{in}-h}$ must meet the total demand distortion (TDD) and harmonic limits up to 50th order specified by IEEE 519 2014 in Table I.

In Table I, I_L is the maximum demand load current and I_{sc} is the short circuit current at the PCC. To meet the current limits of IEEE 519, the following equation must be met

$$
\left| \frac{I_{\text{in}-h}}{I_L} \right| = \left| \frac{\begin{array}{c} V_{\text{ac-CHB-PSPWM}-h}\angle\theta_{\text{PSPWM}-h} \\ + V_{\text{ac-CHB-ASHCM}-h}\angle\theta_{\text{ASHCM}-h} \end{array}}{j\omega_o h L I_L} \right| {\leq} C_h
\tag{10}
$$

where C_h is the limit of the hth order current harmonic in Table I based on the worst short-circuit ratio. Based on IEEE 519 2014, TDD must also meet the standard below

TDD

$$
= \sqrt{\left(\frac{I_{\text{in}-3}}{I_L}\right)^2 + \left(\frac{I_{\text{in}-5}}{I_L}\right)^2 + \cdots + \left(\frac{I_{\text{in}-49}}{I_L}\right)^2} \le C_{\text{TDD}}
\tag{11}
$$

where C_{TDD} is the TDD limit of IEEE 519. It is worth to mention that because [10] addressed the effect of grid voltage harmonics

$$
V_{\text{ac-CHB}-1} = \frac{1}{\sqrt{2}} \sqrt{ \begin{array}{l} (\frac{2V_{\text{dc}}}{\pi}(\cos(\theta_1 - \theta_o) - \cos(\theta_2 - \theta_o) + \cdots - \cos(\theta_k - \theta_o)) + NMV_{\text{dc}}\cos(\theta_o))^2 \\ + (\frac{2V_{\text{dc}}}{\pi}(-\sin(\theta_1 - \theta_o) + \sin(\theta_2 - \theta_o) - \cdots + \sin(\theta_k - \theta_o)) + NMV_{\text{dc}}\sin(\theta_o))^2 \end{array} },
$$

$$
\frac{\sqrt{\begin{array}{l} \left(\frac{4V_{\text{dc}}}{\pi} \sum_{B=1}^{\infty} \left(\sum_{A=-\infty}^{\infty} \left(\frac{1}{2B}J_{2A-1}(NB\pi M)\cos(NB\pi)\sin((2A-1)\theta_o)\right) \right) + \frac{2V_{\text{dc}}}{\pi h}(-\sin(h(\theta_1 - \theta_o)) \right. \\ \left. + \sin(h(\theta_2 - \theta_o)) - \cdots + \sin(h(\theta_k - \theta_o))) \right)^2 \\ + \left(\frac{4V_{\text{dc}}}{\pi} \sum_{B=1}^{\infty} \left(\sum_{A=-\infty}^{\infty} \left(\frac{1}{2B}J_{2A-1}(NB\pi M)\cos(NB\pi)\cos((2A-1)\theta_o)\right) \right) \right. \\ \left. + \frac{2V_{\text{dc}}}{\pi h}(\cos(h(\theta_1 - \theta_o)) - \cos(h(\theta_2 - \theta_o)) + \cdots - \cos(h(\theta_k - \theta_o))) \right)^2 \end{array}}}{|\omega_o h L I_L|} \le C_h, h = 3, 5, 7, \ldots,
$$

$$
\sqrt{\left(\frac{I_{\text{in}-3}}{I_L}\right)^2 + \left(\frac{I_{\text{in}-5}}{I_L}\right)^2 + \cdots + \left(\frac{I_{\text{in}-49}}{I_L}\right)^2} \le C_{\text{TDD}}
\tag{12}
$$

on current harmonics individually, this article will not repeat that work.

Based on (4), (8), (10), and (11), the equation set which is going to be used to calculate switching angles using optimization techniques for the proposed hybrid modulation technique is in (12) shown at the bottom of the previous page.

In (12), the first equation is used to generate the desired fundamental CHB voltage. The second and the third equations are conditions to meet the limits of current harmonics and TDD, respectively. For the sideband harmonics outside the bandwidth defined in (5), because their magnitudes are small, they will be ignored in (12). Only the sideband harmonics within the bandwidth will be considered in (12). Therefore, the number of sideband harmonics of each baseband harmonic in (12) is a function of its bandwidth (5). The switching angles in (12) can be solved using optimization technique such as particle swarm optimization (PSO) technique [19] if critical parameters such as V_{dc}, I_L, K, N, P, and L are determined first.

III. PARAMETER DESIGN FOR THE PROPOSED HYBRID MODULATION TECHNIQUE

In (12), V_{dc}, I_L, K, N, P, and L must be designed for the proposed hybrid modulation technique. To achieve reactive power compensation, the magnitude of the fundamental CHB voltage should be higher than the amplitude of the grid voltage $V_{\text{ac-Grid-1}}$, so

$$\frac{4V_{\text{dc}}(N+P)}{\pi} \geq \sqrt{2}V_{\text{ac-Grid}-1} \Rightarrow V_{\text{dc}} \geq \frac{\sqrt{2}\pi V_{\text{ac-Grid}-1}}{4(N+P)}. \tag{13}$$

I_L is determined based on the maximum volt-ampere of the grid-tied CHB converter. In this article, I_L is 14.1 A, $V_{\text{ac-Grid-1}}$ is 110 V and volt-ampere is 1.56 kVA. Because N cells use the PS-PWM and P cells use the ASHCM-PWM, there is a tradeoff between choosing N and P in different applications. If $N \geq P$, the converter has better a dynamic performance, than $N \leq P$, however, the switching power loss is higher than $N \leq P$, and the inductance which can mitigate the current harmonics is bigger than $N \leq P$. If $N \leq P$, the converter can mitigate more number of current harmonics with lower switching loss than $N \geq P$ while the dynamic performance is not as good as $N \geq P$. If $N + P$ is constant, the design of N and P can start from $N \approx P$. If both the harmonics and the switching power loss can meet the requirements, N can be increased to achieve better desired dynamic response. If one of them could not meet the requirements, P can be increased until meet the requirements. The objective of this article is to use a 3-cell CHB converter to demonstrate that the proposed hybrid modulation technique is better than the conventional PS-PWM technique in meeting harmonic limits with lower switching frequency and smaller L, so $N = 1$ and $P = 2$ are selected. In (5), because $M = 1$, $N = 1$ and $B = 1$, $BW_1 = 10.28f_0$. Based on (6), $f_s > 677$ Hz, so f_s is selected as 720 Hz. So, f_c is 360 Hz and there are 12 switching transitions in each half-period for PS-PWM.

To solve inductance and switching angles from equation set (12) for the desired fundamental and to meet both the current harmonic and TDD limits of IEEE 519, the ranges of K and L should be determined. In (10), for the worst scenario, the harmonic mitigation due to $v_{\text{ac-CHB-ASHCM}-h}$ is ignored, so the biggest inductance L_{worst} is given by (14). Because of the harmonic mitigation due to generated $v_{\text{ac-CHB-ASHCM}-h}$, the
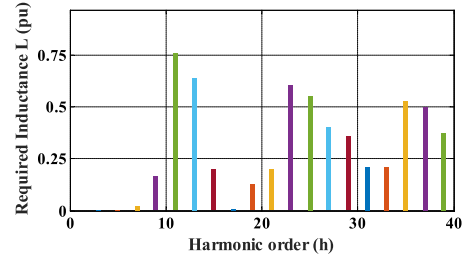

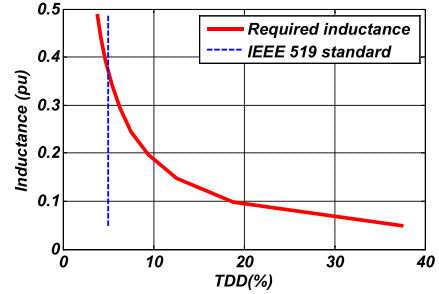Fig. 4. Calculated maximum inductance of each order harmonic based on (14).

Fig. 5. Inductance calculated based on (15).

actual inductance is smaller than L_{worst} as shown in (14)

$$L \leq L_{\text{worst}}$$
$$= \max\left(\frac{|V_{\text{ac-CHB-PSPWM}-h}|}{\omega_o h I_L C_h}\right), \text{ for } h = 3, 5, 7, \cdots \tag{14}$$

Also, to meet TDD limit without the contribution from the ASHCM-PWM, based on (11), inductance L should meet

$$L \geq \frac{1}{C_{\text{TDD}}}\sqrt{\sum_{h=3}^{49}\left(\frac{\max(V_{\text{ac-CHB-PSPWM}-h})}{2\pi h f_o I_L}\right)^2}. \tag{15}$$

Equations (14) and (15) give the range of the inductance L when solving (12). In equation set (12), due to the fact that significant harmonics, which could be over the limit of IEEE 519, of the PS-PWM are within the sidebands of carrier fundamental and harmonics, the low-order voltage harmonics of 60 Hz: 3rd, 5th, . . . , $((f_s - BW_1 - 60)/60)$th, of the PS-PWM are very low in Fig. 2(b). The ASHCM-PWM should mitigate the significant harmonics generated by the PS-PWM within the sidebands of carrier fundamental and harmonics. Fig. 4 shows the highest inductance to meet harmonic limits for each order of harmonics based on (4) and (14). The maximum inductance 0.77 pu happens at 11th order harmonic. Fig. 5 shows the lowest inductances based on (4) and (15) at different TDDs. For 5% TDD in IEEE 519, the inductance is 0.36 pu. If the inductance is within the maximum and lowest values above, the optimization technique can find switching angle solutions to meet (12).

The phasor diagram of (10) is shown in Fig. 6(a) for the hth order harmonic when $|V_{\text{ac-CHB-PSPWM}-h}| \geq |j\omega_o h C_h L I_L|$. $\theta_{\text{PSPWM}-h}$ is from 0 to 2π. To meet the harmonic limit C_h in (10), the end of vector $V_{\text{ac-CHB-ASHCM}-h}$ should always be located within the circle, which centers at the head of vector $V_{\text{ac-CHB-PSPWM}-h}$, with radius $|j\omega_o h C_h L I_L|$. In Fig. 6(b),
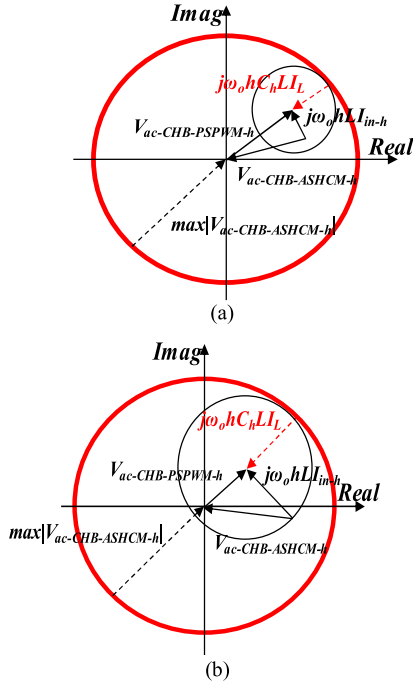
(a)

(b)

Fig. 6. Phasor diagram of (10) for the *h*th order harmonic: (a) when $|V_{\text{ac}-\text{CHB}-\text{PSPWM}-h}| \geq |j\omega_o h C_h L I_L|$ and (b) when $|V_{\text{ac}-\text{CHB}-\text{PSPWM}-h}| < |j\omega_o h C_h L I_L|$.
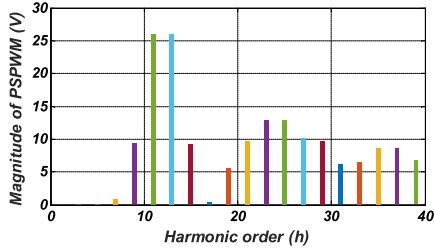

Fig. 7. Maximum magnitudes of the voltage harmonics of the PS-PWM in the normal modulation index range.

when $|V_{\text{ac}-\text{CHB}-\text{PSPWM}-h}| < |j\omega_o h C_h L I_L|$, the magnitude of the $V_{\text{ac}-\text{CHB}-\text{ASHCM}-h}$, no matter what phase it has, only needs to be less than $|j\omega_o h C_h L I_L| - |V_{\text{ac}-\text{CHB}-\text{PSPWM}-h}|$ to meet the current harmonic limit. It is relatively easy to meet the harmonic limit for this case and it has been discussed in [10], so it will not be discussed in this article.

When $|V_{\text{ac}-\text{CHB}-\text{PSPWM}-h}| \geq |j\omega_o h C_h L I_L|$, to meet the harmonic limit for $I_{\text{in}-h}$, based on Fig. 6(a), $|V_{\text{ac}-\text{CHB}-\text{ASHCM}-h}|$ should meet (16)

$$\max\left(|V_{\text{ac}-\text{CHB}-\text{ASHCM}-h}|\right) = \max(|V_{\text{ac}-\text{CHB}-\text{PSPWM}-h}|) + |j\omega_o h C_h L I_L|. \quad (16)$$

At $N = 1$, when the modulation index is within the PS-PWM's normal modulation index range [0, 0.78], the maximum magnitudes of the voltage harmonics of the PS-PWM can be calculated from (4) and are shown in Fig. 7. In Fig. 7, it can be proved that for the case discussed in this section, $|V_{\text{ac}-\text{CHB}-\text{PSPWM}-h}| \geq |j\omega_o h C_h L I_L|$ at the 11th, 13th, 23rd, 25th, 27th, 35th, 37th, and 39th harmonics. So, for these harmonic orders, (16) should be used to design the ASHCM-PWM. Also, the maximum
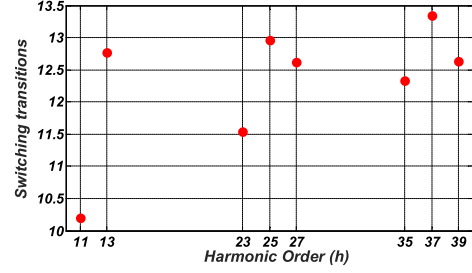

Fig. 8. Calculated maximum number of switching transitions in a half-period for a P-cell ASHCM-PWM.

harmonic magnitude $|V_{\text{ac}-\text{CHB}-\text{ASHCM}-h}|_{\max}$ of the ASHCM-PWM, as proven in [10] is

$$|V_{\text{ac}-\text{CHB}-\text{ASHCM}-h}|_{\max} = \frac{2V_{\text{dc}}K}{\pi h}. \quad (17)$$

Based on (16) and (17), when $|V_{\text{ac}-\text{CHB}-\text{PSPWM}-h}| \geq |j\omega_o h C_h L I_L|$, for the *h*th harmonic, the switching transitions K of the ASHCM-PWM in each half-period should meet the condition below

$$K \leq \frac{\pi h}{2V_{\text{dc}}}(\max|V_{\text{ac}-\text{CHB}-\text{PSPWM}-h}| + |\omega_o h L I_L C_h|). \quad (18)$$

The maximum initial K to solve equation set (12) is given by (18). Fig. 8 shows the maximum switching transitions based on (18) for different harmonic orders. The 37th harmonic requires the highest number of calculated transitions: 13.4. Because 12 is the largest even number below 13.4, the initial K of the ASHCM-PWM to solve (12) should be 12. K should always be an even number and can be further reduced as long as (12) has solutions during the optimization process.

After finding all of these important parameters for (12), for four-quadrant active and reactive power operation in Fig. 1, the desired modulation index M_a and the initial phase θ_o of the CHB voltage are [18]

$$M_a = \left|\frac{\sqrt{2}V_{\text{ac}-\text{Grid}-1}\angle 0 - (R + j\omega_o L)\sqrt{2}I_{\text{in}-1}\angle\theta_{\text{in}}}{4V_{\text{dc}}/\pi}\right| \quad (19)$$

$$\theta_o = \arg\left(\frac{\sqrt{2}V_{\text{ac}-\text{Grid}-1}\angle 0 - (R + j\omega_o L)\sqrt{2}I_{\text{in}-1}\angle\theta_{\text{in}}}{4V_{\text{dc}}/\pi}\right) \quad (20)$$

where θ_{in} is the desired phase of the fundamental ac current and R is the resistance of the inductor. Fig. 9 shows the calculated phases and modulation indices based on (19) and (20) for four-quadrant active and reactive power operation when the magnitude and the phase of the ac current changes between 0 and 20 A, and between 0° and 360°, respectively. To find the solutions of the proposed technique, (12) should be solved by using the optimization techniques.

Different optimization techniques were proposed in literature to solve the equations of low-frequency modulation techniques [2], [4], and [10]. In this article, a PSO technique [19] is used to find the solution of the objective functions in (12). The main principle in evolutionary algorithm such as PSO is to generate random numbers for the constraints of the objective functions to find an optimal solution. In the PSO technique, which is based on the movement of organisms in a fish school and bird flock, the
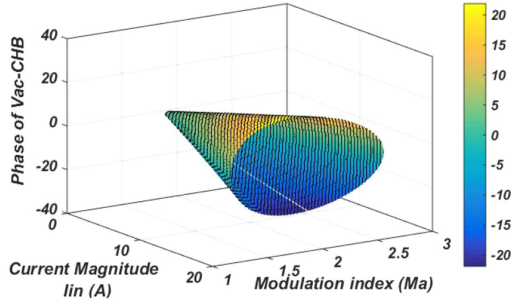
Fig. 9. Solutions of the calculated phase and modulation index for the proposed PS-PWM and ASHCM-PWM technique in four-quadrant active and reactive power operation.

Parameter	Symbol	Value
Line frequency	f_o	60 Hz
AC grid Voltage (RMS)	$V_{ac\text{-}Grid\text{-}1}$	110 V
Total rated power	S_{total}	1.56 kVA
Maximum Demand Load (RMS)	I_L	14.1 A
Switching transitions in each half-period for N=1, P=2,	$N_{PSPWM\text{-}ASHCM}$	22
Switching transitions in each half-period for N=3,	N_{PSPWM}	24
Switching transitions in each half-period for N=3,	N_{SHM}	22
Number of H-bridge cells	I	3
DC bus voltage	V_{dc}	65 V
Coupling inductance	L	0.36pu

particles (switching transitions that should be optimized) of the swarm (all generated random particles in each iteration) should be updated based on the following equations:

$$v_j^{k+1} = wv_j^k + c_1 r_1 (P_{\text{best }j}^k - x_j^k) + c_2 r_2 (G_{\text{best}}^k - x_j^k) \quad (21)$$

$$x_j^{k+1} = x_j^k + v_j^{k+1} \quad (22)$$

where v and x are the velocity and the position of the particles of the swarm; P_{best} is the local best particles of the swarm (the best result of the swarm in the previous iteration) and G_{best} is the global best particles of the swarm in all iterations; r_1 and r_2 are the random numbers; w is the inertia weight; j is the swarm sequence number; and k is the iteration sequence number. The equation set (12) was solved by using PSO to solve the mean square errors of all equations of the objective functions in (12) as shown in (23) shown at the bottom of this page. In (23) the $\lambda_3, ..., \lambda_{\text{TDD}}$ are values between 0 and 1 that are selected by the optimization technique to ensure that all harmonics and the TDD meet the IEEE 519 limits for 3rd, 5th, ..., and TDD, respectively. Also, weight$_1$, weight$_3$, ..., and weight$_{\text{TDD}}$ are weights between 1 and 1000 that are used for fundamental, 3rd, ..., and TDD equations, respectively. The highest weight (1000) in (23), is assigned to the fundamental to ensure that the fundamental is well controlled to the reference value.

In this article, the principle of hybrid PS-PWM and ASHCM-PWM modulation for grid-tied converters is presented. The technique to design critical parameters for the proposed technique is proposed. The technique of achieving good dynamic performance using the proposed hybrid technique will not be investigated here due to limited space but it will be addressed in detail in another paper. The final experimental results will only show the comparison of the dynamic performance but will not be discussed.

The cells with PS-PWM have a greater number of switching transitions than those with ASHCM-PWM so they have higher switching power loss. However, this can be easily solved together with cell power balancing by rotating PS-PWM within all CHB cells in sequence in every period. The dc link voltage balancing has been addressed in other papers such as [20], so it will not be discussed in this article.

IV. EXPERIMENTAL RESULTS

To verify the analysis and advantages of the proposed hybrid PS-PWM and ASHCM-PWM technique, experiments were conducted for a grid-tied 3-cell, 7-level CHB converter. The circuit parameters are shown in Table II and an estimated $0.5\,\Omega$ grid resistance is in series with the grid voltage source. Three experiments were conducted. For the proposed hybrid modulation, one

$$Obj = \left[weight_1 \times \left(V_{ac-CHB-1} - \frac{1}{\sqrt{2}} \sqrt{ \begin{array}{c} \left(\frac{2V_{dc}}{\pi}(\cos(\theta_1 - \theta_o) - \cos(\theta_2 - \theta_o) + \cdots - \cos(\theta_k - \theta_o)) \right. \\ \left. + NMV_{dc}\cos(\theta_o) \right)^2 + \left(\frac{2V_{dc}}{\pi}(-\sin(\theta_1 - \theta_o) \right. \\ \left. + \sin(\theta_2 - \theta_o) - \cdots + \sin(\theta_k - \theta_o)) + NMV_{dc}\sin(\theta_o) \right)^2 \end{array} } \right)^2 \right.$$
$$+ weight_3 \times \left(\frac{\sqrt{ \begin{array}{c} \left(\frac{4V_{dc}}{\pi} \sum_{B=1}^{\infty} \left(\sum_{A=-\infty}^{\infty} \left(\frac{1}{2B} J_{2A-1}(NB\pi M)\cos(NB\pi)\sin((2A-1)\theta_o) \right) \right) \right. \\ \left. + \frac{2V_{dc}}{\pi 3}(-\sin(3(\theta_1 - \theta_o)) + \sin(3(\theta_2 - \theta_o)) - \cdots + \sin(3(\theta_k - \theta_o))) \right)^2 \\ + \left(\frac{4V_{dc}}{\pi} \sum_{B=1}^{\infty} \left(\sum_{A=-\infty}^{\infty} \left(\frac{1}{2B} J_{2A-1}(NB\pi M)\cos(NB\pi)\cos((2A-1)\theta_o) \right) \right) \right. \\ \left. + \frac{2V_{dc}}{\pi 3}(\cos(3(\theta_1 - \theta_o)) - \cos(3(\theta_2 - \theta_o)) + \cdots - \cos(3(\theta_k - \theta_o))) \right)^2 \end{array} }}{|3\omega_o L I_L|} - \lambda_3 C_3 \right)^2$$
$$\left. + \cdots + weight_{TDD} \times \left(\sqrt{ \left(\frac{I_{in-3}}{I_L} \right)^2 + \left(\frac{I_{in-5}}{I_L} \right)^2 + \cdots + \left(\frac{I_{in-49}}{I_L} \right)^2 } - \lambda_{TDD} C_{TDD} \right)^2 \right]^{1/2}$$
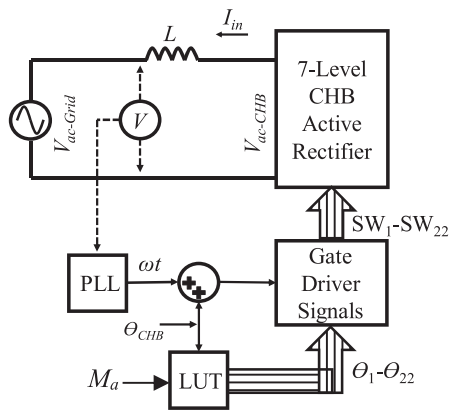
$$(23)$$

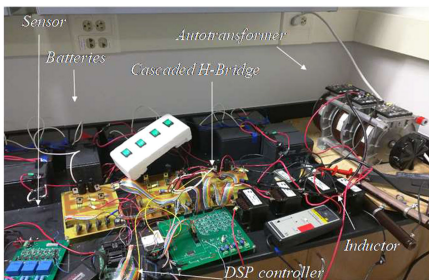Fig. 10. Function block diagram of a 7-level CHB converter in experiments.

Fig. 11. Hardware prototype of the 7-level grid-tied CHB converter.

cell uses PS-PWM with 12 switching transitions in a half-period as calculated in Section III. Two cells use ASHCM-PWM with switching transitions $K = 10$ (the switching angle solutions were found based on (12) after K is reduced from initial 12 to 10) in a half-period. The total number $N_{\text{PSPWM-ASHCM}}$ of switching transitions of the CHB converter is therefore 22 in half period. For comparison, conventional PS-PWM and SHM-PWM techniques are also applied to three cells and the total number N_{PSPWM} of switching transitions in half period is 24 ($f_s = 24 \times 60 = 1.44$ kHz) based on (5) and (6). Also, the same number of switching transitions as the proposed ASHCM-PWM technique are applied to the conventional SHM-PWM technique (N_{SHM}) in experiments. It should be noted that the general equation sets (12) and (23) can be applied to any number of cells with the PS-PWM and ASHCM-PWM technique. In the experiments, to show the proposed hybrid technique can meet the power quality standard with lower number of switching angles than the conventional PS-PWM technique, two cells use ASHCM-PWM technique and one cell uses PS-PWM technique.

A 3-cell, 7-level grid-tied CHB converter with the same parameters as in Table II is developed with the function block in Fig. 10. Also, the hardware prototype of the proposed hybrid technique with the 7-level CHB converter is shown in Fig. 11. A lookup table is used to store switching angles which were solved offline from (12). It should be pointed out that although this article focuses on the modulation technique for grid-tied converters, the proposed technique is not limited by power level. The 1.56 kVA power in Table II does not invalidate the advantages of the proposed technique in possible high-power applications. The TMS320F28335 digital signal processor (DSP) is used in the experiments to control H-bridge cells. In the first experiment, the average modulation index of all cells of the CHB

TABLE III
SWITCHING ANGLES OF THE PROPOSED HYBRID PSPWM AND ASHCM-PWM TECHNIQUE

Switchings	Fig.12 (f)	Fig. 13 (f)	Fig. 14 before transient	Fig. 14 after transient
Θ_1	+74	+93	+102	+83
Θ_2	-148	-161	+73	+54
Θ_3	+52	+24	-89	-91
Θ_4	+97	+122	+37	+20
Θ_5	-119	-104	-117	-155
Θ_6	+142	+146	+17	+41
Θ_7	-159	-73	-161	-57
Θ_8	-92	-139	+50	+108
Θ_9	+17	+64	-32	-33
Θ_{10}	-63	-126	-58	-111

converter is 0.52, and the total modulation index of the converter is 1.57. The phase of the CHB fundamental voltage is -21.2. The active and reactive power is 1.39 kW + 0.63 kVAR. Fig. 12(a), (d), and (f) shows the time-domain waveforms of the grid-tied CHB converter with the conventional SHM-PWM (quarter-wave symmetry), conventional PS-PWM, and the proposed hybrid modulation technique, respectively. Fig. 12(b) and (c) shows the voltage harmonic and the current harmonic spectra of the conventional SHM-PWM, respectively. As shown in the figures, although the conventional SHM-PWM technique can meet the individual voltage harmonic limits of IEEE 519 [the red line in Fig. 12(b)], it cannot meet the THD requirement ($\leq 8\%$), the current harmonic limits at 3rd, 23rd, 35th, and 43rd orders [red line in Fig. 12(c)] and TDD ($\leq 5\%$) which are the important requirements for the grid-tied converters. Fig. 12(e) and (g) shows the current harmonic spectra of the conventional PS-PWM technique and the proposed hybrid modulation technique. The red lines in Fig. 12(e) and (g) are the current harmonic limits of IEEE 519. As shown in Fig. 12(e), the 19th, 23rd, 25th, 29th, and 55th current harmonics cannot meet the limits of IEEE-519 with the conventional PS-PWM. The TDD in Fig. 12(e) cannot meet the limits of IEEE 519 ($\leq 5\%$) too due to the voltage harmonics of the actual power grid, low-switching frequency of the PS-PWM technique, and the small timing errors of switching transitions introduced by the DSP. This problem can be solved by applying the asymmetric switching angle control technique in [21] to the proposed hybrid PS-PWM and ASHCM-PWM technique. In this technique, the magnitudes and phases of the CHB voltage harmonics are controlled incorporating the information from the grid voltage harmonics to meet the TDD limits. As shown in Table II and Fig. 12(g), even with a smaller number of switching transitions than conventional PS-PWM, the proposed hybrid modulation can meet all current harmonic limits up to 100th order (IEEE 519 requirements are up to 50th). The switching angles of the proposed hybrid technique in Fig. 12(f) are shown in Table III. The + and − signs in front of each switching angle represent the positive polarity (a cell generates $+V_{\text{dc}}$) or the negative polarity (a cell generates $-V_{\text{dc}}$) at the switching angle. Fig. 12(h) shows the required inductance of the PS-PWM technique at different harmonics to meet the current harmonic requirements of the IEEE 519. Around 1.22 pu inductance should be used with the conventional PS-PWM technique to meet the current harmonic limits. For the conventional SHM-PWM as proved in
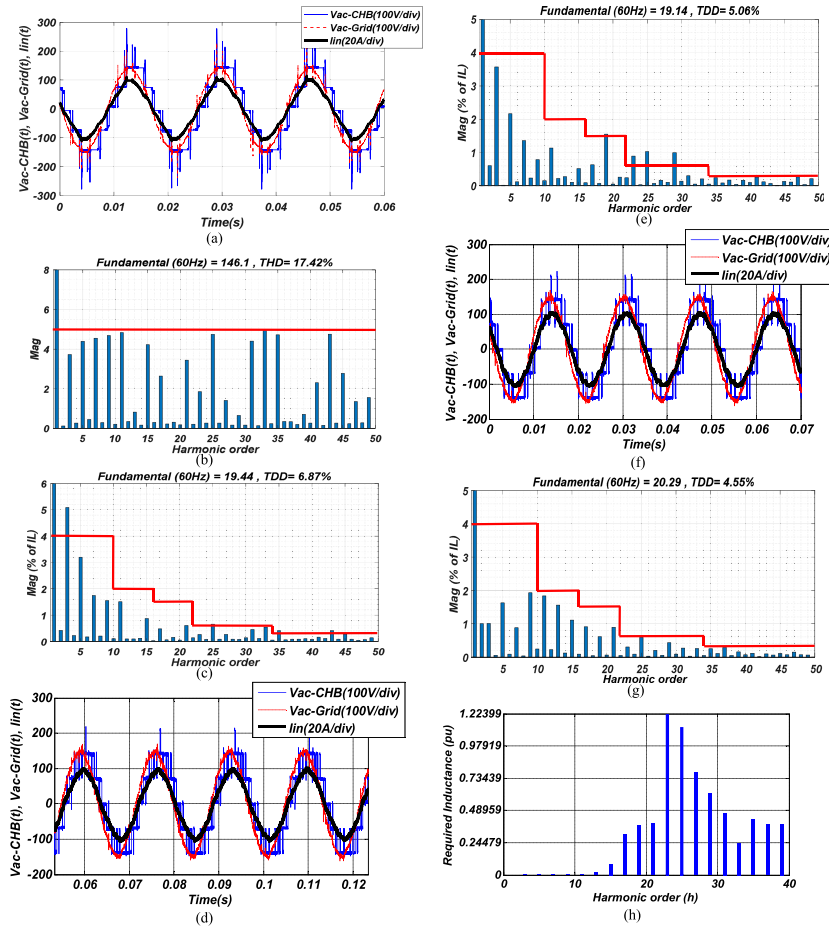
Fig. 12.   Waveforms and current harmonic spectra of $v_{\text{ac-CHB}}(t)$, $v_{\text{ac-Grid}}(t)$, and $i_{\text{in}}(t)$, when $M = 0.52$ and $\theta_0 = -21.2$, (a) time-domain waveform of the conventional SHM-PWM technique, (b) harmonic spectra of $v_{\text{ac-CHB}}(t)$ for the conventional SHM-PWM, (c) harmonic spectra of $i_{\text{in}}(t)$ for the conventional SHM-PWM, (d) time domain waveform of conventional PS-PWM technique, (e) harmonic spectra of $i_{\text{in}}(t)$ for the conventional PS-PWM technique, (f) time-domain waveform of the proposed hybrid modulation technique, (g) harmonic spectra of $i_{\text{in}}(t)$ for the proposed technique, (h) required inductance of the conventional PS-PWM to meet the current harmonics.

[10], the required inductance to meet the current harmonics is much higher than the SHCM-PWM technique which is used in this article.

In the second experiment, the average modulation index M of all cells is 0.69 so the total modulation index Ma of the CHB converter is 2.096. The phase of the CHB fundamental voltage is -3.2. The active and reactive power is 0.57 kW + 0.03 kVAR. Fig. 13(a), (d), and (f) shows the time-domain waveforms of the CHB converter with the conventional (quarter-wave symmetry) SHM-PWM, the conventional PS-PWM, and the proposed hybrid modulation techniques, respectively. Fig. 13(b) and (c) show the voltage harmonic and the current harmonic spectra of the CHB converter with the conventional SHM-PWM technique, respectively. It is shown that the SHM-PWM technique in Fig. 13(b) can meet the individual voltage harmonic limits of IEEE 519 but not the THD requirement. In Fig. 13(c), it cannot meet the current harmonic limits at 3rd, 35th, 37th, 49th orders and the TDD limit which are the important requirements for the grid-tied converters. Also, Fig. 13(e) and (g) show the current harmonic spectra of the conventional PS-PWM and the proposed hybrid modulation techniques. In Fig. 13(e), the conventional PS-PWM technique cannot meet limits for the 17th, 23rd, 25th, 27th, and 31st harmonics. The proposed hybrid modulation technique in Fig. 12(g) meets all current harmonic limits. The TDDs of both techniques meet the TDD limit of IEEE 519. The

switching angles of the proposed hybrid technique in Fig. 13(f) are shown in Table III.

In the last experiment, the transient response of the proposed hybrid modulation when current (both active and reactive) changes from $7.62\angle33.8°$A to $6.18\angle-36°$A with 0.48 pu inductance was tested in Fig. 14. It has only 6.8% dc offset and almost zero settling time. The current also meets the harmonic limits before and after the transient. This transient free performance can be achieved with timing control for both active and reactive currents. The proposed technique thus has no dynamic performance issue. Due to the limited space here, the transient free technique will be addressed in detail in another paper. The switching angles of all switching transitions in Fig. 14 are given in Table III for both before and after the transient.

As shown in experimental results in this article, the proposed hybrid technique has the following benefits compared with the conventional SHM-PWM and PS-PWM techniques: a) with a lower number of switching transitions (22 switching transitions in each half-period) than the conventional PS-PWM (24 switching transitions in each half-period), it can meet the harmonic limits of IEEE 519 for the grid-tied converters (the conventional PS-PWM cannot meet the limits); b) also, the proposed hybrid PS-PWM and ASHCM-PWM technique can meet the current harmonic limits which is impossible for the conventional quarter-wave symmetry SHM-PWM technique; c)
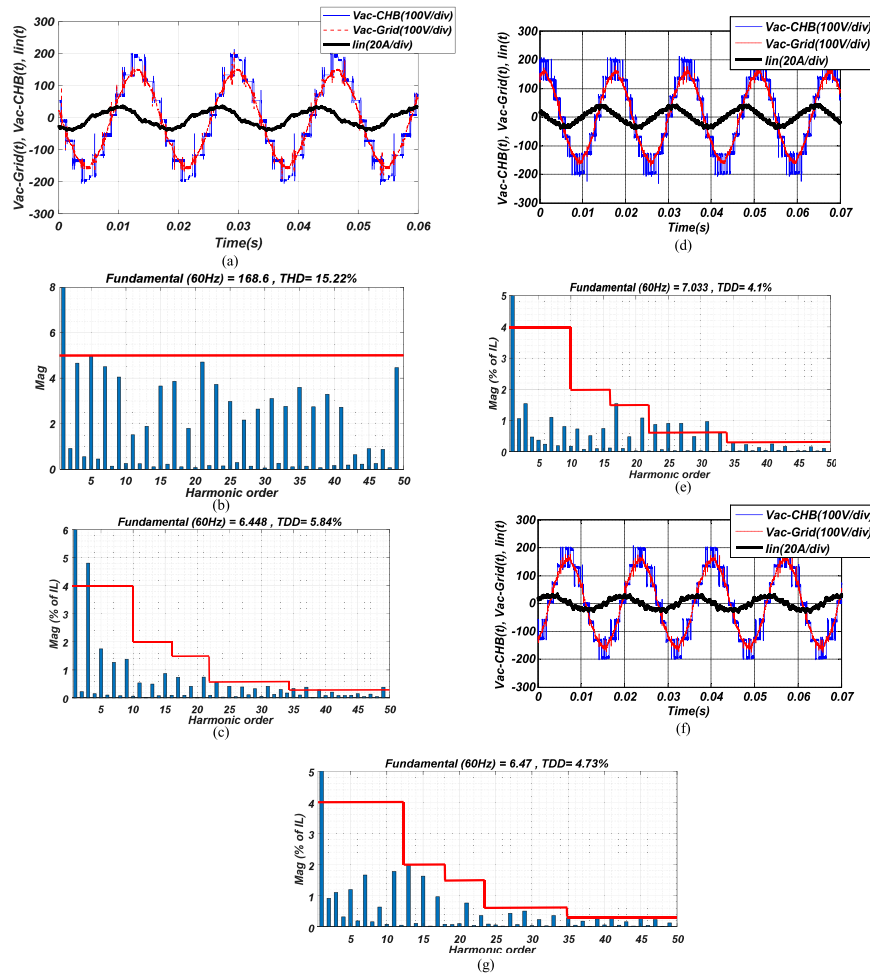
Fig. 13. Waveforms and current harmonic spectra of $v_{\text{ac-CHB}}(t)$, $v_{\text{ac-Grid}}(t)$, and $i_{\text{in}}(t)$ when $M = 0.69$ and $\theta_0 = -3.2°$: (a) time-domain waveform of the conventional SHM-PWM technique, (b) harmonic spectra of $v_{\text{ac-CHB}}(t)$ of the conventional SHM-PWM, (c) harmonic spectra of $i_{\text{in}}(t)$ of the conventional SHM-PWM, (d) time domain waveform of conventional PS-PWM technique, (e) harmonic spectra of $i_{\text{in}}(t)$ for the conventional PS-PWM technique, (f) time-domain waveform of the proposed hybrid modulation technique, (g) harmonic spectra of $i_{\text{in}}(t)$ for the proposed technique.
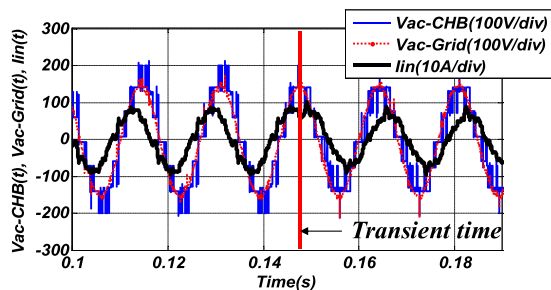

Fig. 14. Dynamic response of the proposed hybrid modulation technique.

as shown in Fig. 12(h), the conventional PSPWM technique requires 1.22 pu inductance to meet all low order current harmonic limits, while the proposed hybrid technique just require 0.36 pu inductance; d) from the current harmonic spectrum of the conventional SHM-PWM and the analysis in paper [10], it has been proved that the proposed technique requires smaller inductance than the conventional SHM-PWM technique; (e) the proposed hybrid modulation also aschieves better dynamic performance than conventional SHM-PWM.

V. CONCLUSION

This article proposed a hybrid PS-PWM and ASHCM-PWM technique for cascaded multilevel converters. The technique utilized ASHCM-PWM to mitigate the harmonics generated from PS-PWM to meet harmonic limits with a smaller number of switching transitions and smaller inductance than the conventional PS-PWM technique. Also, the proposed technique showed a better performance than the conventional SHM-PWM technique in terms of meeting the current harmonic limits, smaller inductance, and better dynamic response. Design technique were developed for critical parameters, such as coupling inductance and the number of switching transitions, for the proposed hybrid PS-PWM and ASHCM-PWM technique. Simulations and experiments were conducted to validate the proposed technique.

REFERENCES

[1] S. Khomfoi and L. M. Tolbert, "Multilevel power rectifiers," in *Power Electronics Handbook*. Knoxville, TN, USA: Butterworth-Heinemann, 2011, pp. 455–486.

[2] M. Dahidah, G. Konstantinou, and V.G. Agelidis, "A review of multilevel selective harmonic elimination PWM: Formulations, solving algorithms, implementation and applications," *IEEE Trans. Power Electron.*, vol. 30, no. 8, pp. 4091–4106, Aug. 2015.

[3] A. J. Watson, P. W. Wheeler, and J. C. Clare, "A complete harmonic elimination approach to dc link voltage balancing for a cascaded multilevel rectifier," *IEEE Trans. Ind. Electron.*, vol. 54, no. 6, pp. 2946–2953, Dec. 2007.

[4] L. G. Franquelo, J. Napoles, R. C. P. Guisado, J. I. Leon, and M. A. Aguirre, "A flexible selective harmonic mitigation technique to meet grid codes in three-level PWM rectifiers" *IEEE Trans. Ind. Electron.*, vol. 54, no. 6, pp. 3022–3029, Dec. 2007.

[5] D. G. Holmes and T. A. Lipo. *Pulsewidth Modulation for Power Converters: Principles and Practice*, Hoboken, NJ, USA: Wiley, 2003.

[6] Li Li, D. Czarkowski, L. Yaguang, and P. Pillay, "Multilevel selective harmonic elimination PWM technique in series-connected voltage inverters," *IEEE Trans. Ind. Appl.*, vol. 36, no. 1, pp. 160–170, Jan./Feb. 2000.

[7] A. Moeini, H. Iman-Eini, and A. Marzoughi, "DC link voltage balancing approach for cascaded H-bridge active rectifier based on selective harmonic elimination-pulsewidth modulation," *IET Power Electron.*, vol. 8, no. 4, pp. 583–590, Apr. 2015.

[8] M. Sharifzadeh, H. Vahedi, R. Portillo, L. G. Franquelo, and K. Al-Haddad, "Selective harmonic mitigation based self-elimination of triplen harmonics for single-phase five-level inverters," *IEEE Trans. Power Electron.*, vol. 34, no. 1, pp. 86–96, Jan. 2019.

[9] M. Aleenejad, H. Mahmoudi, P. Moamaei, and R. Ahmadi, "A new fault-tolerant strategy based on a modified selective harmonic technique for three-phase multilevel converters with a single faulty cell," *IEEE Trans. Power Electron.*, vol. 31, no. 4, pp. 3141–3150, Apr. 2016.

[10] A. Moeini, H. Zhao, and S. Wang, "A current-reference-based selective harmonic current mitigation PWM technique to improve the performance of cascaded H-bridge multilevel active rectifiers," *IEEE Trans. Ind. Electron.*, vol. 65, no. 1, pp. 727–737, 2016.

[11] A. Semedyarov and A. Ruderman, "Selective harmonic mitigation by time domain constrained optimization," in *Proc. 9th IEEE Int. Symp. Power Electron. Distrib. Gener. Syst.*, Charlotte, NC, USA, 2018, pp. 1–6.

[12] A. Khamitov, A. Semedyarov, R. Polichshuk, and A. Ruderman, "Time domain constrained optimization of low switching frequency synchronous modulation for a two-level three-phase inverter," in *Proc. IEEE 18th Int. Power Electron. Motion Control Conf.*, Budapest, Hungary, 2018, pp. 1038–1042.

[13] C. Yonggang, P. Wang, L. Yaohua, L. Zixin, and T. Longcheng, "A novel hybrid modulation method for cascaded H-bridge active power filter," in *Proc. 13th Int. Power Electron. Motion Control Conf.*, Poznan, Poland, 2008, pp. 1981–1986

[14] A. Moeini, Z. Hui, and S. Wang, "High efficiency, hybrid selective harmonic elimination phase-shift PWM technique for cascaded H-bridge inverters to improve dynamic response and operate in complete normal modulation indices," in *Proc. IEEE Appl. Power Electron. Conf. Expo.*, Long Beach, CA, USA, 2016, pp. 2019–2026.

[15] M. Miranbeigi and H. Iman-Eini, "Hybrid modulation technique for grid-connected cascaded photovoltaic systems," *IEEE Trans. Ind. Electron.*, vol. 63, no. 12, pp. 7843–7853, Dec. 2016.

[16] *IEEE Recommended Practices and Requirements for Harmonic Control in Electrical Power Systems*, IEEE Std 519-2014 (Revision of IEEE Std 519-1992), New York, NY, USA, Jun. 11, 2014, pp. 1–29.

[17] A. Kumar and V. Verma, "Performance enhancement of single-phase grid-connected PV system under partial shading using cascaded multilevel converter," *IEEE Trans. Ind. Appl.*, vol. 54, no. 3, pp. 2665–2676, May/Jun. 2018.

[18] A. Moeini, H. Zhao, and S. Wang, "Improve control to output dynamic response and extend modulation index range with hybrid selective harmonic current mitigation-PWM and phase-shift PWM for four-quadrant cascaded H-bridge converters," *IEEE Trans. Ind. Electron.*, vol. 64, no. 9, pp. 6854–6863, Sep. 2017.

[19] R. Eberhart and J. Kennedy, "A new optimizer using particle swarm theory," in *Proc. Sixth Int. Symp. Micro Mach. Human Sci.*, Nagoya, Japan, 1995, pp. 39–43.

[20] A. Moeini and S. Wang, "A cascaded hybrid phase shift-PWM and asymmetric selective harmonic mitigation-PWM modulation technique for grid-tied converter to reduce the switching frequency and meet the grid current harmonic requirement," in *Proc. IEEE Appl. Power Electron. Conf. Expo.*, Tampa, FL, USA, 2017, pp. 3486–3493.

[21] A. Moeini and S. Wang, "Asymmetric selective harmonic elimination technique using partial derivative for cascaded modular active rectifiers tied to a power grid with voltage harmonics," in *Proc. Asia-Pacific Int. Symp. Electromagn. Compat.*, Shenzhen, China, 2016, pp. 982–987.

[22] A. Moeini and S. Wang, "A dc link sensor-less voltage balancing technique for cascaded H-bridge multilevel converters with asymmetric selective harmonic current mitigation-PWM," *IEEE Trans. Power Electron.*, vol. 33, no. 9, pp. 7571–7581, Sep. 2018.

[23] H. Iman-Eini, J. Schanen, S. Farhangi, and J. Roudet, "A modular strategy for control and voltage balancing of cascaded H-bridge rectifiers," *IEEE Trans. Power Electron.*, vol. 23, no. 5, pp. 2428–2442, Sep. 2008.

[24] H. Zhao, T. Jin, S. Wang, and L. Sun, "A real-time selective harmonic elimination based on a transient-free inner closed-loop control for cascaded multilevel inverters," *IEEE Trans. Power Electron.*, vol. 31, no. 2, pp. 1000–1014, Feb. 2016.

Amirhossein Moeini (S'16–M'19) received the Ph.D. degree in electrical engineering from the University of Florida, Gainesville, FL, USA, in 2019.

He is currently a Postdoctoral Research Fellow with the Department of Electrical and Computer Engineering with the Missouri University of Science and Technology, Rolla, MO, USA. He has authored or coauthored more than 25 journal and conference papers and holds two USA patents. His current research interests include power electronics, multilevel converters, deep/machine learning, battery management, and EV charging stations.
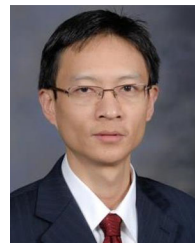
Shuo Wang (S'03–M'06–SM'07–F'19) received the Ph.D. degree in electrical engineering from Virginia Tech, Blacksburg, VA, USA, in 2005.

He is currently a Full Professor with the Department of Electrical and Computer Engineering, University of Florida, Gainesville, FL, USA. He has authored or coauthored more than 180 IEEE journal and conference papers and holds around 30 pending/issued US/international patents.

Dr. Shuo Wang received the Best Transaction Paper Award from the IEEE Power Electronics Society in 2006 and two William M. Portnoy Awards for the papers published in the IEEE Industry Applications Society in 2004 and 2012, respectively. In 2012, he received the prestigious National Science Foundation CAREER Award. He is an Associate Editor for the IEEE TRANSACTIONS ON INDUSTRY APPLICATIONS and a Technical Program Cochair for the IEEE 2014 International Electric Vehicle Conference.
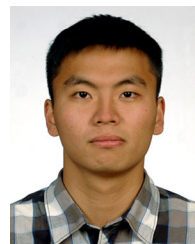
Boyi Zhang (S'17) received the B.S degree in electrical engineering from the Harbin Institute of Technology, Harbin, China, in 2015, and the M.S. degree in electrical and computer engineering in 2017 from the University of Florida, Gainesville, FL, USA, where is currently working toward the Ph.D. degree with the Power Electronics and Electrical Power Research Lab, University of Florida.

He has authored and coauthored several IEEE conference and transaction papers. His research interests include electromagnetic interference, wide bandgap power device packaging, and magnetic components.

Mr. Zhang received the Best Student Presentation Award in the Applied Power Electronics Conference (APEC) in 2017 and 2019.

Le Yang (S'16) received the B.S. degree from Xi'an Jiaotong University, Shaanxi, China, in 2012, and the M.S. degree from the Huazhong University of Science and Technology, Wuhan, China, in 2015, both in electrical engineering. He is currently working toward the Ph.D. degree in power electronics with the Power Electronics and Electrical Power Research Lab, University of Florida, Gainesville, FL, USA.

His current research interests include electromagnetic interference modeling and suppression techniques in grid-tied power converters systems and motor drive systems, and magnetic components integration techniques.